Wideband Acoustic Microscopy of Tissue

CHRISTOPHER M. W. DAFT AND G. A. D. BRIGGS

Abstract—**A scanning acoustic microscope (SAM) has been used to measure the elastic properties of tissue with a resolution of around 8 μm. This is achieved by broad-band excitation of the acoustic lens, and the recording of an undemodulated returning signal. A method of analyzing this information to yield the sound velocity, acoustic impedance, section thickness and acoustic attenuation is described. Results from a sample of skin tissue are presented and compared with data from a computer simulation of the experiment.**

I. Introduction

IT HAS been noted [1] that the scientific basis of acoustic scattering by human tissue has received little attention until recently. The realization that important diagnostic capabilities may arise from a more basic knowledge of the acoustic properties of tissue has prompted the use of various techniques [2]–[4] for such measurements. In this paper it is shown how a scanning acoustic microscope (SAM) may be employed to provide this data with greater resolution than has previously been available.

In a typical high-frequency-reflection SAM [5] the lens is excited by a relatively narrow-band toneburst, and images of sections of tissue can be produced in pseudotransmission by mounting the tissue on a glass slide, and focussing on the tissue/glass interface. The problem with these images is that with at least four sources of contrast (impedance, thickness, velocity and attenuation), more information than the peak height of the returning echo is needed. While ways of obtaining the phase of this signal have already been described [6],[7] a direct determination of the contrast mechanism requires a different approach.

In this paper, the effects of exciting the lens with a voltage spike from a step recovery diode are examined. This approach is common at frequencies up to 100 MHz [8], and the resolution of such systems has been predicted [9]. A higher frequency range (100–500 MHz) can be combined with the impulse excitation technique in order to yield sufficient time resolution to separate the reflections from the two boundaries of a 10–15-μm histological section. Fig. 1(a) shows the signal from the lens without tissue, and Fig. 1(b) is a trace recorded from a typical section.

Manuscript received February 18, 1988. This work was supported in part by SERC and in part by the GEC Hirst Research Center.

C. M. W. Daft is with the Bioacoustics Research Laboratory, Department of Electrical and Computer Engineering, University of Illinois, 1406 West Green Street, Urbana, IL 61801

G. A. D. Briggs is with the Department of Metallurgy and Science of Materials, Oxford University, Parks Road, Oxford OX1 3PH, England

IEEE Log Number 8824737.

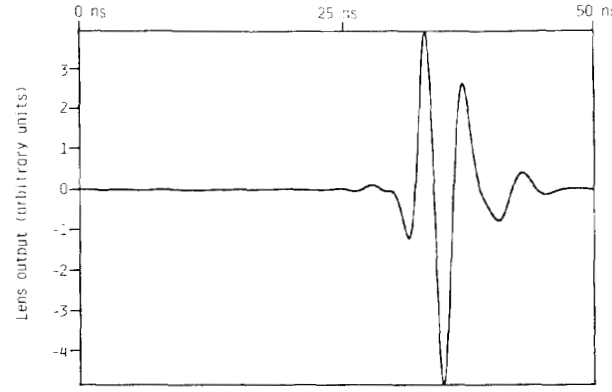

Fig. 1a. Signal from glass slide only.

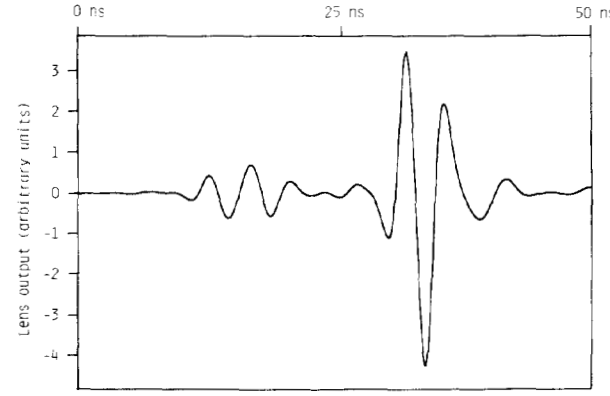

Fig. 1b. Signal from tissue on glass slide.

II. Computer Simulation of the Experiment

The quasi-CW (continuous wave) imaging theory of the acoustic microscope is well developed [10]–[12]. This was extended to the broad-band case in order to simulate the experiment and check the validity of the analysis.

The response of an acoustic lens at a single frequency has been calculated using Fourier optics [10]:

$$V = C \int_0^{\theta_H} P(\theta)\, R(\theta) \exp\left[j 2kz \cos\theta \right] \cos\theta \sin\theta \, d\theta \tag{1}$$

where:

V	lens output;
θ_H	lens semiangle;
$P(\theta)$	pupil function of the lens;
$R(\theta)$	reflection coefficient of the object;
k	$2\pi/\lambda_{\text{water}}$;
C	numerical constant; and
z	defocus of lens.

The first task is therefore to calculate $R(\theta)$. Fig. 2 shows the geometry of the situation. Snell's law requires that

$$\frac{\sin \theta_W}{v_W} = \frac{\sin \theta_T}{v_T} = \frac{\sin \theta_S}{v_S} = \frac{\sin \theta_L}{v_L} \tag{2}$$

where v_W, v_T, v_S, and v_L are the velocities in the water, tissue and substrate (shear and longitudinal). Oliner [13] has devised a method whereby a layered acoustic system may be reduced to a simple network of transmission lines, transformers, and terminating impedances. Fig. 3 is the circuit analogue for this case. The tissue is represented by a transmission line of length t and characteristic impedance

$$Z_T = \frac{\rho_T v_T}{\cos \theta_T} \tag{3}$$

where ρ_T is the tissue density.

Acoustic energy incident on the glass is transferred into shear and longitudinal waves. These modes are symbolized by the two transformers, with turns ratios given by

$$n_1 = \frac{k_{sz}^2 - k_{sx}^2}{k_s^2} = \cos 2\theta_S \tag{4}$$

$$n_2 = \frac{2k_{sx}k_{sz}}{k_s^2} = \sin 2\theta_S \tag{5}$$

where the wavenumber notation is the same as that used in [13]. The terminating impedances are

$$Z_1 = \frac{\rho_G v_L}{\cos \theta_L} \tag{6}$$

$$Z_2 = \frac{\rho_G v_S}{\cos \theta_S} \tag{7}$$

where ρ_G is the glass density. The transformers and impedances are combined into a single terminating impedance Z_{TER}:

$$Z_{TER} = n_1^2 Z_1 + n_2^2 Z_2. \tag{8}$$

An expression for the input impedance for the complete circuit can then be written down as

$$Z_{IN} = Z_T \frac{\exp(jkt) + C \exp(-jkt)}{\exp(jkt) - C \exp(-jkt)} \tag{9}$$

where

$$C = \frac{Z_{TER} - Z_T}{Z_{TER} + Z_T} \tag{10}$$

and

$$k = \frac{2\pi f}{v_T} - j\alpha(f). \tag{11}$$

In (11), $\alpha(f)$ denotes the attenuation of the tissue. The reflectance of the tissue/glass combination is given by

$$R(\theta) = \frac{Z_{IN} - Z_W}{Z_{IN} + Z_W} \tag{12}$$

where Z_W is the acoustic impedance of water.

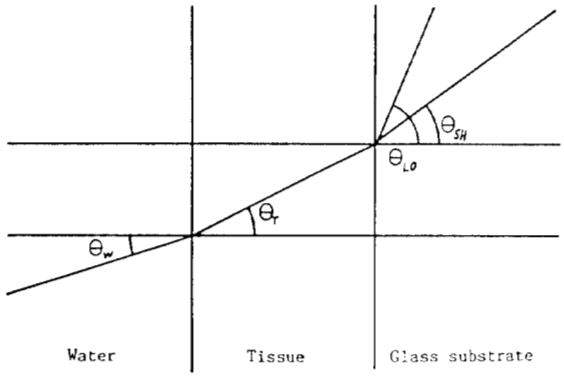

Fig. 2. Geometry of plane waves in tissue imaging experiment.

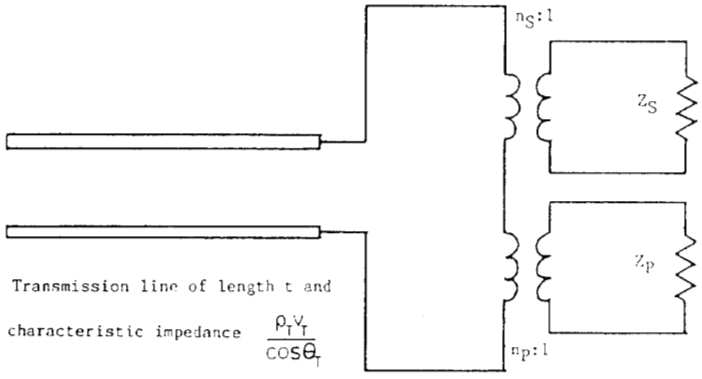

Fig. 3. Equivalent circuit.

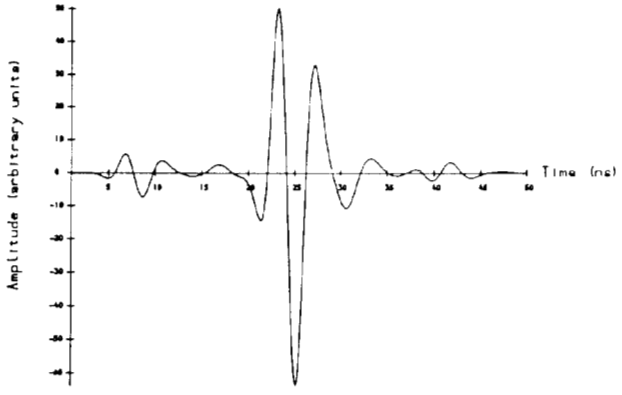

Fig. 4. Typical simulated $V(t)$.

The least satisfactory aspect of this way of simulating the experiment is the fact that $P(\theta)$ cannot be measured accurately at these frequencies. The function

$$P(\theta) = \exp\left[-(\theta/\theta_0)^2\right] - \exp\left[-(\theta_H/\theta_0)^2\right] \tag{13}$$

was chosen, with $\theta_H = 50°$ and $\theta_0 = 25°$, to approximate to the lens used in the experiments. In this expression, the first term is a Gaussian function of standard deviation $\theta_0/\sqrt{2}$. The integral (1) is only evaluated for $0 < \theta < \theta_H$, since no sound is emitted from the lens at higher angles of incidence. The second (constant) term was added so that $P(\theta_H) = 0$. $P(\theta)$ has been measured at 10 MHz for a focused transducer [11]. The lens used in this experiment includes a buffer section between a planar trans-

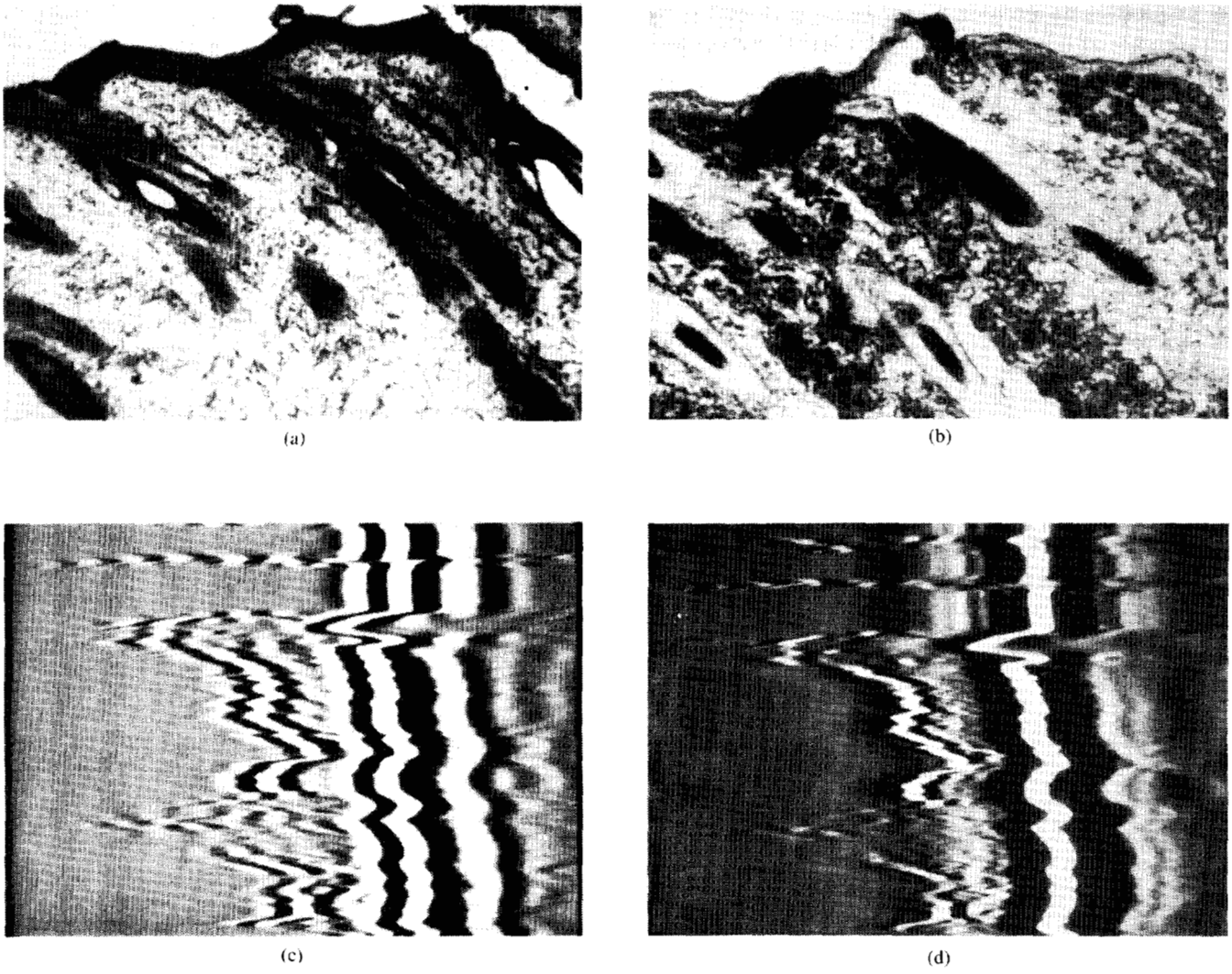

Fig. 5. Results obtained with skin section. (a) Optical image (1.4-μm field-of-view (FOV)). (b) SAM image (730-μm FOV). (b) SAM image (730-μm FOV). (c) Time resolved linescan (705-μm FOV). (d) Wiener filtered linescan (705 μm fov).

ducer and a spherical focusing surface, that may have a very different $P(\theta)$.

The broad-band aspect of the experiment was modelled by digitizing a trace obtained with the glass in position but without tissue. This was Fourier transformed into an estimate of the incident spectrum $M(f)$. The spectrum was a smoothly varying function with center frequency 250 MHz, and adequate signal-to-noise ratio (SNR) from 100 to 500 MHz. Tissue properties were then chosen and $V(f)$ computed. The result was then obtained by an inverse transform

$$V(t) = \int M(f)\, V(f) \exp(-j2\pi ft)\, df. \quad (14)$$

A simulated trace calculated in this way is shown in Fig. 4. The first pulse visible is the reflection from the surface of the tissue. Its size is determined by the tissue acoustic impedance, and its position by the thickness of the tissue. The second pulse, in the center of the trace, is the tissue/glass signal. This pulse is considerably larger than the first one, because of the large difference in impedance between the tissue and its glass substrate. The trace has been scaled to the reference signal obtained without tissue. Thus, the size of the second pulse gives an indication of the tissue attenuation. If the tissue velocity increases, this pulse will move to the left, since the time of flight in the tissue will decrease. The third signal is from the double round trip path in the tissue; it has not been used in the calculation of tissue properties.

III. Experimental Measurements

A guinea pig was sacrificed and blocks dissected from the skin of the back of the animal were frozen in freon cooled by liquid nitrogen. Sections were cut transverse to the plane of the skin surface in a Lipshaw cryostat, and mounted unfixed on glass slides. These specimens were imaged conventionally in the SAM at 425 MHz, using a 60 ns toneburst and a receiver bandwidth of 10 MHz. These parameters ensure that the two echoes from the surfaces of the tissue are completely mixed, since the time-

of-flight through the section is typically 20 ns. Time resolution data was recorded for one line of the toneburst image. Other sections were stained with toluidene blue and imaged in a transmission optical microscope. Details of the experimental arrangement can be found in [14]. In summary, the lens is excited by an impulse in order to interrogate the tissue with the shortest possible acoustic signal. The undemodulated echoes are detected with a sampling oscilloscope; signal averaging and background subtraction are then used to enhance the measurement accuracy. However, the sampling process severely reduces the rate of data collection. Consequently, images of the elastic properties were not feasible. Instead, a line scan through the center of the SAM image is recorded. This also has the advantage that the raw data can be displayed as a *B*-scan image.

Fig. 5 shows the images obtained. The optical image (Fig. 5(a)) is illustrative of the type of structures contained in this tissue, but is not of the same area as the acoustic data. The epidermis (the superficial dark layer) is visible, and beneath it the dermis makes up most of the image. Cells are continuously exfoliated from the skin surface, and are replaced by cells which arise from mitotic activity in the basal layer of the epidermis. As they move upwards they elaborate keratin, which has acoustic properties markedly different from other tissues. The dermis contains collagen fibers running more or less parallel to the skin surface. It has been suggested [15] that the collagen-containing components of tissue are largely responsible for contrast in clinical *B*-scanning. Between these fibers are positioned elastic fibers, sebaceous glands, sweat glands, and hair follicles. The hairs and hair follicles are visible in Fig. 5(a).

Fig. 5(b) shows the appearance of the section in the SAM, operating in toneburst mode, with the focal plane 7 μm above the glass surface. The epidermis appears to be less attenuating than much of the dermis; a lighter shade of grey in the images denotes an increase in transmission of ultrasound. Hairs, which have a high concentration of keratin, appear very dark.

The lens was positioned at the center of the horizontal scan, and scanned along a line running from the top to the bottom of Fig. 5(b) while the time resolution data was collected. The result is shown in Fig. 5(c), in which the horizontal axis represents time (50 ns total width) and the vertical axis is distance. Picture brightness is proportional to detected voltage, so the no-signal level is grey and a pulse train (such as in Fig. 3) appears as a number of black and white stripes. The right-hand (brighter) pulse is the tissue–glass signal, and the left-hand pulse is the tissue–water signal. The reflection from the top surface of the tissue is stronger here than for many other tissue types, due to the high concentration of structural protein.

IV. Analysis of Data

As a first step in analyzing the data of Fig. 5(c), the pulses were shortened by the application of a Wiener filter [16]. If the signal from the tissue is denoted by $s(t)$, and $r(t)$ is a reference signal obtained with the lens at the same vertical position but without tissue, the Wiener filter output in the frequency domain is

$$W(f) = \frac{S(f)\,R^*(f)}{R(f)\,R^*(f) + N^2} \tag{15}$$

where $S(f)$ and $R(f)$ are the Fourier transforms of $s(t)$ and $r(t)$, $*$ denotes a complex conjugate, and N^2 is a constant which depends on the system noise level. The effect of this filter on the data is shown in Fig. 5(d).

In order to calculate the tissue elastic properties, equations modelling the signal were devised. It was simpler to do this in the frequency domain:

$$R(f) = M(f) \exp(2\pi f t_3) \tag{16}$$

$$S(f) = AM(f) \exp(2\pi j f t_1) + \alpha(f)\, M(f) \exp(2\pi j f t_2) \tag{17}$$

where A is a real constant, $\alpha(f)$ is a real function representing the frequency dependence of the tissue attenuation and two way transmission loss, and t_1, t_2, and t_3 are the arrival times of the tissue/water, tissue/glass and reference signals respectively.

Since it is assumed that the first (tissue/water) pulse has the same shape as the reference pulse, its position and amplitude were found using a correlation technique. The function

$$C(\tau) = \frac{\int s(t)\, r(t+\tau)\, dt}{\int r^2(t)\, dt} \tag{18}$$

was computed, and its maximum value found, $C_{MAX}(\tau_{MAX})$. A quadratic fit to the top three points was made. Then

$$A = C_{MAX} \tag{19}$$

$$t_1 - t_3 = \tau_{MAX}. \tag{20}$$

It can be shown [17] that this formula is an unbiased and efficient estimator of these quantities. The impedance Z_T and thickness x are then found from

$$Z_T = Z_W \frac{1 + A}{1 - A} \tag{21}$$

$$x = v_W(t_1 - t_3)/2. \tag{22}$$

The function

$$U(f) = \left|S(f)/R(f)\right|^2 - A^2 \tag{23}$$

is computed, which from (16) and (17) is equal to

$$\alpha^2(f) + 2A\alpha(f) \cos 2\pi f(t_1 - t_2). \tag{24}$$

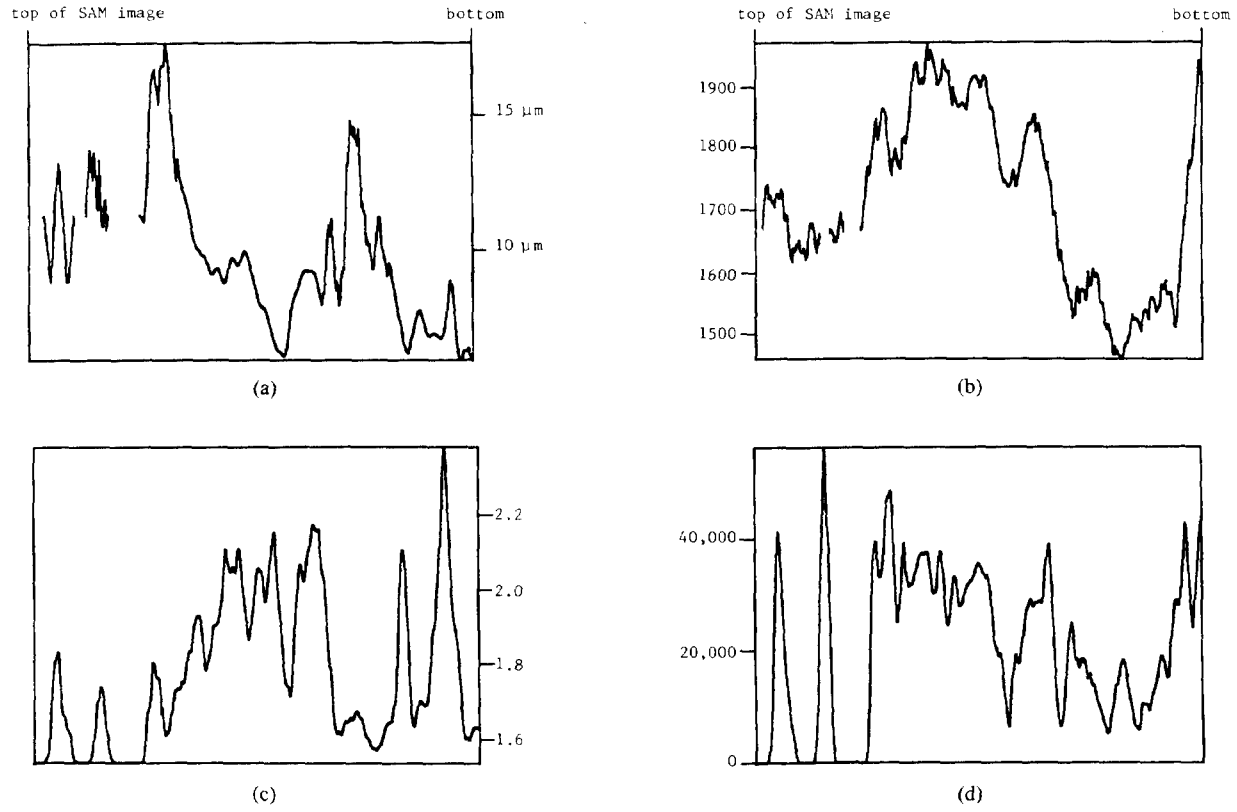

Fig. 6. Elastic properties of skin section. (a) Thickness (μm). (b) Velocity (ms^{-1}). (c) Impedance (MRayl). (d) Averaged attenuation ($Np\ m^{-1}$).

A mean squared attenuation is calculated by averaging this function over the frequency range

$$\overline{\alpha^2} = \frac{\int U(f)\,df}{f_{MAX} - f_{MIN}}. \tag{25}$$

This is then converted to a value in NP m^{-1} after removing the two way transmission loss (computed from the acoustic impedance at that point).

The velocity is computed by a method akin to homomorphic deconvolution [18]. A straight line is fitted by the least-squares method to $U(f)$ and subtracted to yield a waveform centered around the frequency axis. This is then Hamming windowed [19] and transformed back to the time domain. The peak of this trace is $t_1 - t_2$, which is related to the tissue velocity by

$$v_T = 2x/(t_1 - t_2). \tag{26}$$

The consistency of this method of modelling the experiment was tested by generating data with the simulation described in Section II, and feeding the waveforms into the analysis program. Tissue parameters were varied widely, and the percentage difference between the parameter specified and that calculated by the analysis was taken. The sensitivity of the method to the shape of $P(\theta)$ was examined by varying the standard deviation parameter θ_0 in (14) from 0.3° to 30°. In all cases, the thickness estimate was accurate to 0.2 percent, and the velocity error was less than 1 percent. It appears that neither of these is strongly dependent on $P(\theta)$. The velocity error may largely be caused by estimating the center frequency of a necessarily truncated signal $[U(f)]$ with a Fourier transform. Leakage of negative frequency data into the main peak changes the position of the maximum. The acoustic impedance error shows a more marked dependance on half angle, varying from 1 percent at $Z_T = 1.6$ MRayl to 10 percent at $Z_T = 2.05$ MRayl. This reflects the limited validity of the assumption that the first pulse is a scaled and time-shifted replica of the reference pulse. Dispersion, which makes v_T and Z_T dependent on frequency, has been assumed to be negligible in the present work. This is discussed further in [20]. For comparison, the experimental errors caused principally by temperature drift in the coupling fluid, and deviations from a perfectly flat lens scan, produce 5-percent errors in thickness, and hence velocity measurements.

The results of applying this analysis to the data of Fig. 5 are shown in Fig. 6. These graphs represent the variations in elastic properties down the center of the image of Fig. 5(b). A wider range of elastic properties than is typical in lower frequency studies can be seen. In the attenuation linetrace (Fig. 6(d)), two peaks corresponding to the epidermis and a hair are visible. A high velocity is observed in the vicinity of the hair, which appears as a large dark object near the center of Fig. 5(b). This is due to its high structural protein content. The attenuation and

impedance remain fairly high throughout the section, which reflects the presence of collagen and keratin.

V. Conclusion

The use of very short, wideband pulses enables the various contributions to a SAM image of tissue to be measured. The thickness, sound velocity, impedance and attenuation data can be computed from the time domain response of the microscope when the lens is excited by an impulse. A similar technique has been utilized at 100 MHz [21] to provide depth resolution in images of the backscatter from living tumor spheroids.

The elastic properties of tissue vary more substantially on a microscopic scale than is the case macroscopically. This is an unsurprising conclusion, since a larger sound wavelength would tend to average out fine structure in the elastic parameters. There is also a correlation between areas of high velocity and high attenuation. This is consistent with the trends observed by Johnston *et al.* [22], who drew together the available ultrasonic data on many different types of tissue. In general, as the tissue/water content decreases, and the structural protein content increases, the speed of sound and attenuation both increase.

Further work in this area will concentrate on investigating other types of tissue [23], and examining the frequency dependence of the tissue attenuation [20].

Acknowledgment

We are grateful to Dr. D. M. Shotton and Dr. J. Carnwath for help with tissue preparation, and Drs. M. G. Somekh, J. M. R. Weaver and J. M. Rowe for invaluable discussions.

References

[1] C. R. Hill, R. C. Chivers, R. W. Huggins, and D. Nicholas, "Scattering of ultrasound by human tissue," in *Ultrasound: Its Applications in Medicine and Biology*, F. J. Fry, Ed. Amsterdam: Elsevier, 1978, pp. 441-493.

[2] P. M. Embree, S. G. Foster, G. Bright, and W. D. O'Brien, "Ultrasonic velocity spatial distribution analysis of biological materials with the scanning laser acoustic microscope," in *Acoustical Imaging, Vol. 13*, M. Kaveh, R. K. Mueller, and J. F. Greenleaf, Eds. New York: Plenum, 1984, pp. 203-216.

[3] D. A. Sinclair and I. R. Smith, "Tissue characterization using acoustic microscopy," in *Acoustical Imaging, Vol. 12*, E. A. Ash and C. R. Hill, Eds. New York: Plenum, 1982, pp. 505-516.

[4] F. S. Foster, M. Strban, and G. Austin, "The ultrasound macroscope: Initial studies of breast tissue," *Ultrason. Imaging*, vol. 6, pp. 243-261, 1984.

[5] A. Atalar and M. Hoppe, "High-performance acoustic microscope," *Rev. Sci. Instrum.*, vol. 57, no. 10, pp. 2568-2576, 1986.

[6] K. K. Liang, S. D. Bennett, B. T. Khuri-Yakub, and G. S. Kino, "Precise phase measurements with the acoustic microscope," *IEEE Trans. Sonics Ultrason.*, vol. SU-32, no. 2, pp. 266-273, Mar. 1983.

[7] C. M. W. Daft, J. M. R. Weaver, and G. A. D. Briggs, "Phase contrast imaging of tissue in the scanning acoustic microscope," *J. Microsc.*, vol. 139, no. 3, pp. RP3-RP4, 1985.

[8] K. Yamanaka, "Surface acoustic wave measurements using an impulsive converging beam," *J. Appl. Phys.*, vol. 54, no. 8, pp. 4323-4329, 1983.

[9] M. Nikoonahad and E. A. Ash, "Resolution of scanning ultrasonic imaging systems with arbitrary transducer excitation," *Rev. Phys. Appl.*, vol. 20, pp. 383-389, 1985.

[10] C. J. R. Sheppard and T. Wilson, "Effects of high angles of convergence on $V(z)$ in the scanning acoustic microscope," *Appl. Phys. Lett.*, vol. 38, no. 11, pp. 858-859, 1981.

[11] K. K. Liang, G. S. Kino, and B. T. Khuri-Yakub, "Material characterization by the inversion of $V(z)$," *IEEE Trans. Sonics Ultrason.*, vol. SU-32, no. 2, pp. 213-225, Mar. 1985.

[12] C. Chou and G. S. Kino, "The evaluation of $V(z)$ in a type II reflection microscope," *IEEE Trans. Ultrason. Ferroelec. Freq. Contr.*, vol. UFFC-34, no. 3, pp. 341-345, May 1987.

[13] A. A. Oliner, "Microwave network methods for guided elastic waves," *IEEE Trans. Microwave Theory Tech.*, vol. MTT-17, no. 11, pp. 812-826, Nov. 1969.

[14] J. M. R. Weaver, C. M. W. Daft, and G. A. D. Briggs, "Crack characterization with the scanning acoustic microscope," submitted for publication to *IEEE Trans. Ultrason. Ferroelec. Freq. Contr.*

[15] W. D. O'Brien, Jr., "The role of collagen in determining ultrasonic propagation properties in tissue," in *Acoustic Holography, Vol. 7*, L. W. Kessler, Ed. New York: Plenum Press 1977, pp. 37-50.

[16] Y. Murakami, B. T. Khuri-Yakub, G. S. Kino, J. M. Richardson, and A. G. Evans, "An application of Wiener filtering to nondestructive evaluation," *Appl. Phys. Lett.*, vol. 33, no. 8, pp. 685-687, 1978.

[17] A. D. Whalen, *Detection of Signals in Noise*. London: Academic, 1971, 332f.

[18] L. E. Roemer, C. Chen, and M. S. Hostetler, "Cepstral processing using spread spectra for cable diagnostics," *IEEE Trans. Instrum. Meas.*, vol. IM-30, no. 1, pp. 31-37, Jan. 1981.

[19] A. V. Oppenheim and R. W. Schafer, *Digital Signal Processing*. Englewood Cliffs, N.J.: Prentice Hall, 1975, pp. 239-250.

[20] C. M. W. Daft, G. A. D. Briggs, and W. D. O'Brien, Jr., "Frequency dependence of tissue attenuation measured by acoustic microscopy," submitted to *J. Acoust. Soc. Am.*

[21] M. D. Sherar, M. B. Noss and F. S. Foster, "Ultrasound backscatter microscopy images the internal structure of living tumor spheroids," *Nature*, vol. 330, pp. 493-495, 1987.

[22] R. L. Johnston, S. A. Goss, V. Maynard, J. F. Brady, L. A. Frizzell, W. D. O'Brien, Jr., and F. Dunn, "Elements of tissue characterization," in *Ultrasonic Tissue Characterization II*, M. Linzer, Ed. Washington: U.S. Gov. Printing Office, NBS Spec. Publ. 525, 1979, pp. 19-27.

[23] C. M. W. Daft and G. A. D. Briggs, "The elastic microstructure of various tissues," *J. Acoust. Soc. Am*, in press.

Christopher M. W. Daft was born in Dundee, Scotland, in 1963, and received the B.A. and D. Phil. degrees from Oxford University in 1984 and 1987, respectively.

In 1987 he joined the Bioacoustics Research Laboratory of the Department of Electrical and Computer Engineering at the University of Illinois, Champaign-Urbana, as a Visiting Assistant Professor. His research interests include acoustic microscopy and tissue characterization.

G. A. D. Briggs received his B.A. degree in physics at Oxford University, Oxford, England, in 1971 and his Ph.D. degree in physics at Cambridge University, Cambridge, England in 1976.

In 1980 he returned to Oxford to develop applications of acoustic microscopy to materials science. In 1982 he was appointed Royal Society Research Fellow in the Physical Sciences, and in 1984 he became a Lecturer in Metallurgy at Oxford University and a Fellow of Wolfson College at Oxford. He is on the Council of the Royal Microscopical Society and Chairman of the Materials Section, and he has written the Royal Microscopical Society Handbook on Acoustic Microscopy.